Data-Driven Gas Sensing Analysis of Tin Sulfide Films Modified with Copper

Hayim Ch. Magid[1], Muna Ahmed Issa[2], Z. M. Shabanb[1], Shaymaa A. Hussein[3], Sami Salman Chiad[1], Nadir Fadhil Habubi[1, 4, 5] and Yassin Hasan Kadhim[6]

[1]*Department Department of Physics, College of Education, Mustansiriyah University, 10052 Baghdad, Iraq*
[2]*Quality Assurance and Performance Evaluation Department, Mustansiriyah University, 10052 Baghdad, Iraq*
[3]*Department of Medical Laboratory Techniques, Al-Manara College for Medical Sciences, 62001 Amarah, Iraq*
[4]*Department of Radiation and Sonar Technologies, Alnukhba University College, 10001 Baghdad, Iraq*
[5]*Department of Radiology Techniques, Al-Qalam University College, 36001 Kirkuk, Iraq*
[6]*Department of Optics Techniques, College of Health and Medical Techniques, Al-Mustaqbal University, 51001 Hillah, Iraq*
halhelfy@uomustansiriyah.edu.iq, muna.ahmed@uomustansiriyah.edu.iq, Zinam.shaban@uomustansiriyah.edu.iq, shaimaa2021@uomanara.edu.iq, dr.sami@uomustansiriyah.edu.iq, nadirfadhil@uomustansiriyah.edu.iq, yassin.hasan@uomus.edu.iq

Keywords: Sns, Cu, Plasma Jet, XRD, Optical Properties, Topography, E_g, Sensitivity, Resistance.

Abstract: Considerable attention was paid to the physical characteristics of SnS:Cu thin films produced by plasma jet technique at different argon flow rates of 0.5, 1, and 1.5 L/min. According to XRD patterns, the grown films are cubic polycrystalline with a dominating peak at the (115) plane. The investigation guarantees that the structure and dominating peak were unaffected by varying the flow rate. The XRD profile shows an increase in grain size (nm) from 11.25 nm to 12.36 nm as the argon flow rate increases. Similarly, the strain decreased from 30.81 x 10-4 to 28.04 x 10-4 with increasing flow rate. Using atomic force microscopy, the average particle size was determined to be between 88.1 and 42.3 nm, while the average roughness was between 10.69 and 3.26 nm. SEM analysis of films prepared at different flow rates revealed distinct trends. Films prepared at 0.5 L/min exhibited higher aggregation and a more homogeneous structure. Whereas those prepared at 1-1.5 L/min showed increased porosity. In Vis-NIR areas, the transmission values of the films exceed 75%. The absorption coefficient increased with increasing argon flow rate, while the optical energy gap values decreased from 1.42 eV to 1.30 eV. Additionally, optical constants decreased as the flow rate increased. SnS:Cu films show decreased resistance with higher argon flow, indicating improved crystallinity, surface uniformity, and enhanced charge carrier mobility. SnS:Cu films show decreasing NO_2 sensitivity with higher argon flow rates.

1 INTRODUCTION

Over the past two decades, tin monosulfide (SnS) has garnered significant attention due to its myriad optoelectronic applications [1]-[3]. Early investigations, such as Hoffman's work in 1935, delved into the orthorhombic structure of SnS. This structure comprises layers of Sn and S atoms, held together by weak van der Waals-type bonding between layers [4]. Notably, SnS compounds exhibit a wide band gap ranging from 1.2 to 1.6 eV [5], [6]. The absorption coefficient of these compounds is sufficiently high, reaching up to 104 cm^{-1}, making them suitable for applications as absorber layers [7], [8]. Researchers have employed various techniques to produce SnS thin films, including sol-gel [9], spray pyrolysis [10], electrodeposition [11], EBE [12], SILAR [13], PLD [14], CBD [15], and RF-magnetron sputtering [16]. The plasma jet technique is a relatively new process for the synthesis of nanostructured thin films that provides several attractive features such as the formation of very reactive species at atmospheric pressure, facilitating rapid and highly controllable reactions, and encouraging the development of desired composition and morphology of the films within controlled parameters that give the plasma jet technique its effectiveness and versatility as technology [17]-[19]. This study aims to get more information about the structural, morphological, and optical properties as a function of argon flow rate for the prepared films.

These studies are indispensable for deepening the knowledge of SnS: Cu nanostructures and enhancing their performance in optoelectronic and sensing devices.

2 EXPERIMENTAL

SnS: Cu thin films were synthesized using an atmospheric pressure plasma jet system. In this work, argon gas was used as the working gas with different flow rates of 0.5, 1.0, and 1.5 L/min to investigate the effect of gas flow on the properties of the films. The plasma nozzle was positioned 2 cm above the surface of 10 mL of deionized water containing tin chloride ($SnCl_2$) as the tin source and thiourea ($(NH_2)_2CS$) as the sulfur precursor. Additionally, copper chloride ($CuCl_2$) was added to the solution to introduce copper into the SnS matrix. During plasma operation, the interaction of the high-energy argon plasma plume with the precursor solution generated reactive species that initiated chemical reactions, resulting in the formation of SnS:Cu nanoparticles directly in the liquid phase. To study the effect of gas flow rate, all other synthesis conditions were kept constant, with only the flow rate varied. The gradual change in the color of the colloidal suspensions confirmed formation of nanoparticles. The obtained SnS:Cu nanoparticles were deposited on pre-cleaned glass substrates using the drop-casting technique. The deposited films were allowed to dry naturally at room temperature, forming visible thin layers on the substrate surface. These as-deposited films were subsequently annealed in a laboratory furnace at 150 °C for 30 minutes to enhance densification, surface uniformity, and adhesion. After annealing, the films were subjected to XRD, AFM, and UV–Vis characterization. The resulting SnS:Cu thin films exhibited a compact, homogeneous structure and strong adhesion to the substrate, confirming the effectiveness of the plasma jet. Gas sensitivity measurements are generally performed in a cylindrical testing chamber with a radius of 7.5 cm and a height of 15 cm.

3 RESULTS AND DISCUSSIONS

The crystallographic characteristics of the deposited films are presented in Figure 1 through their X-ray diffraction (XRD) patterns. The observed diffraction peaks located at 38.41°, 45.02°, 50.24°, and 63.12° are indexed to the (113), (105), (115), and (220) planes, respectively [20]. These reflections are consistent with ICDD card No. 34-1439, confirming the crystalline nature of the synthesized films. The presence of well-defined peaks indicates that all samples exhibit a polycrystalline structure. Among them, the (115) reflection at $2\theta = 50.24°$ is the most dominant feature. It is also observed that the intensity of this peak increases with increasing argon flow rate, suggesting that deposition conditions significantly influence crystal orientation and enhance overall film crystallinity [18].

The crystallite size (D) was estimated using Scherrer's equation [21], [22]. The calculated values, as summarized in Table 1, are 11.25 nm, 11.70 nm, and 12.36 nm for films deposited at argon flow rates of 0.5, 1.0, and 1.5 L/min, respectively. The gradual increase in crystallite size with flow rate indicates that higher gas flow promotes improved atomic arrangement and crystal growth during deposition. Larger crystallites are generally associated with better structural ordering and enhanced crystallinity [23], [24].

The dislocation density (δ) was evaluated using the standard relation [25], [26]. The results show a decrease in δ from 79.01 to 65.45 as the argon flow rate increases from 0.5 to 1.5 L/min. This reduction suggests that higher flow rates contribute to fewer crystallographic defects within the lattice. Lower dislocation density is typically indicative of improved structural quality and increased stability of the films [27], [28].

The lattice strain (ε) was calculated using the corresponding relation [29], [30]. A decreasing trend is observed, where strain reduces from 30.81 to 28.04 with increasing argon flow rate. This decline reflects reduced lattice distortion and indicates the formation of a more relaxed crystal structure. The simultaneous decrease in both strain and dislocation density confirms the improvement in crystalline quality with increasing flow rate [18]. The overall structural parameters are summarized in Table 1, while their variation with flow rate is illustrated in Figure 2.

Atomic force microscope (AFM) micrographs and roughness analysis are presented in Figure 3 (a_1 - c_3). The 3-D images and particle size (P_{av}) are depicted in Figure 3 (a_1, b_1, and c_1), showing spherical nano-grains with sizes ranging from 42.3 nm to 88.1 nm at a flow rate of 1.5 L/min. The increase in copper doping led to a rise in average surface roughness (R_a) due to the increase in grain size. The findings indicate that increasing copper doping leads to a refinement in the surface morphology, resulting in smaller and more uniform nano-grains [31]. The AFM parameters, visually represented in Figure 3 and

quantified in Table 2, provide a comprehensive analysis of the impact of copper doping on the observed surface characteristics of the SnS films.

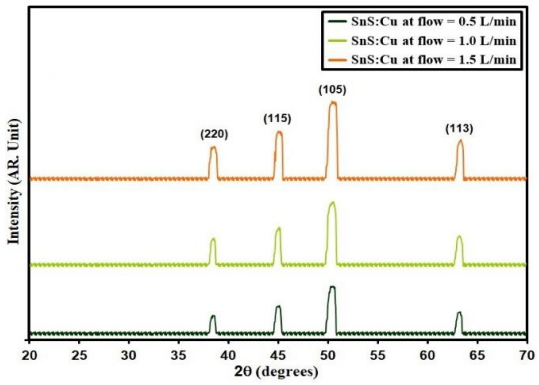

Figure 1: XRD styles of the prepared films.

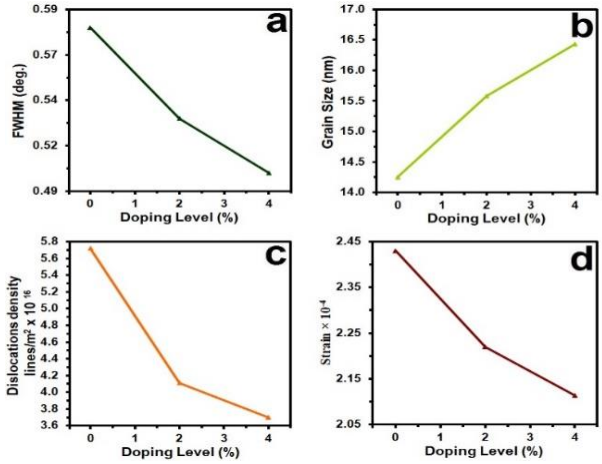

Figure 2: P_{st} of SnS: Cu films.

Table 1: D, E_g, and P_{st} of SnS: Cu films.

Specimen	2 q (º)	(hkl) Plane	FWHM (º)	E_g (eV)	*D* (nm)	δ (× 10^{14}) (lines/m^2)	Ɛ (× 10^{-4})
SnS: Cu at flow= 0.5 L/min	50.24	115	0.78	1.42	11.25	79.01	30.81
SnS: Cu at flow= 1 L/min	20.21	115	0.75	1.38	11.70	73.05	29.63
SnS: Cu at flow= 1.5 L/min	50.20	115	0.71	1.30	12.36	65.45	28.04

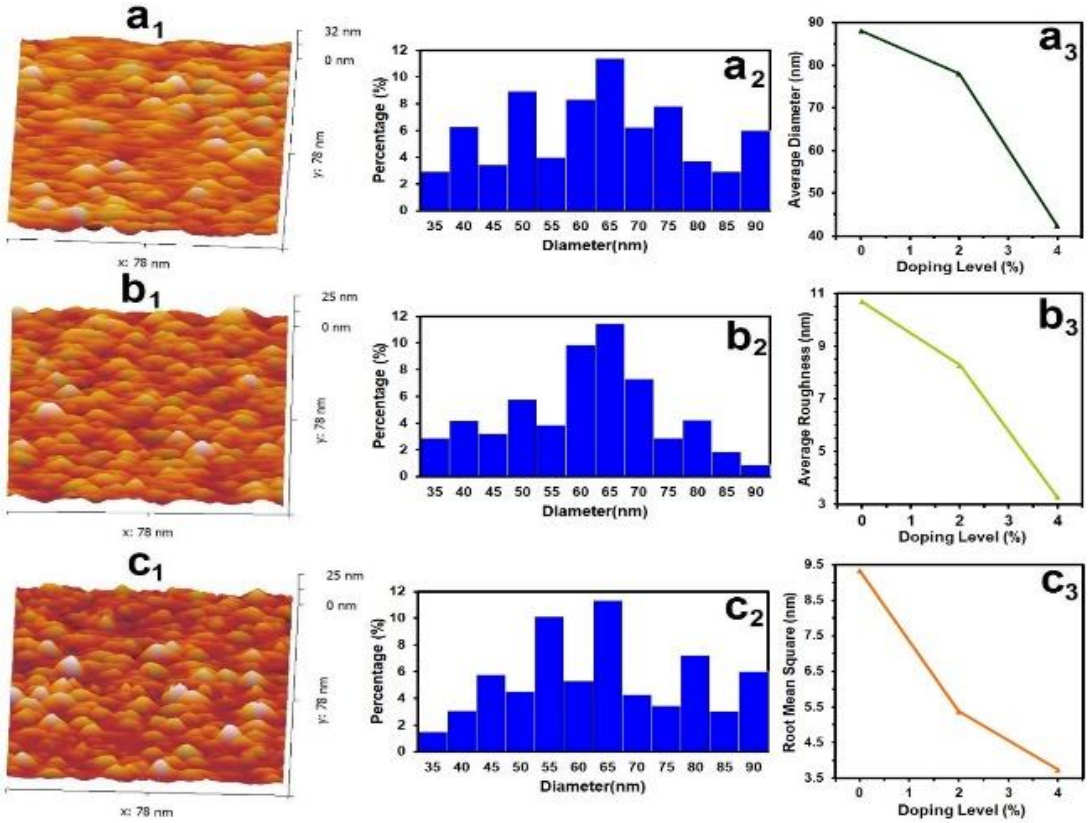

Figure 3: AFM of SnS: Cu films.

Table 2: P_{AFM} of SnS: Cu films.

Samples	Pav nm	Ra (nm)	Rrms (nm)
SnS: Cu at flow= 0.5 L/min	42.3	3.26	3.73
SnS: Cu at flow= 1 L/min	78.0	8.28	5.38
SnS: Cu at flow= 1.5 L/min	88.1	10.69	9.34

The optical transmittance of the deposited films was evaluated using the standard definition of percentage transmittance [32], [33], where it is expressed as the ratio of transmitted to incident light intensity. Here, I_0corresponds to the incident light intensity and Irepresents the transmitted intensity after passing through the film. The transmittance results shown in Figure 4 reveal the optical behavior of films prepared under different argon flow rates. The sample grown at the lowest flow rate (0.5 L/min) exhibits relatively high transparency, reaching up to 75%. In contrast, a gradual reduction in optical transmission is observed as the flow rate increases to 1.0 and 1.5 L/min. This decrease indicates that the deposition conditions strongly influence the optical transparency of the SnS:Cu films [32]. The reduction in transmittance at higher flow rates can be attributed to enhanced plasma–solution interactions, which alter the microstructure and increase light scattering and absorption within the film [34], [35].

The absorption coefficient (α) was determined from the optical absorbance data using the established relation [36], [37], which incorporates film thickness as a key parameter. The variation of α is presented in Figure 5. The results show that the absorption coefficient increases with increasing argon flow rate. This behavior suggests that stronger plasma interaction during deposition modifies the electronic structure of the SnS:Cu films, leading to higher light absorption. Such an increase may be associated with changes in defect states and density of states within the material, which enhance photon absorption. Similar trends have been reported in previous studies, where increased plasma activity led to higher absorption coefficients due to structural and electronic modifications [38], [39].

Using Tauc's relation, the optical bandgap (Eg) of the deposited films was determined from the absorption data [40], [41]. This approach relates the absorption coefficient and photon energy, where A is a material-dependent constant and hν represents the incident photon energy. The obtained results, presented in Figure 6, show a gradual decrease in Eg from 1.42 eV at 0.5 L/min to 1.30 eV at 1.5 L/min. This reduction in bandgap energy with increasing argon flow rate can be associated with improvements in crystallinity and an increase in particle size, both of which influence the electronic structure of the films [42], [43].

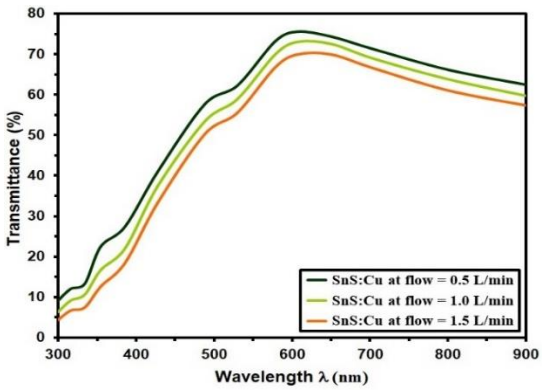

Figure 4: T of SnS: Cu films.

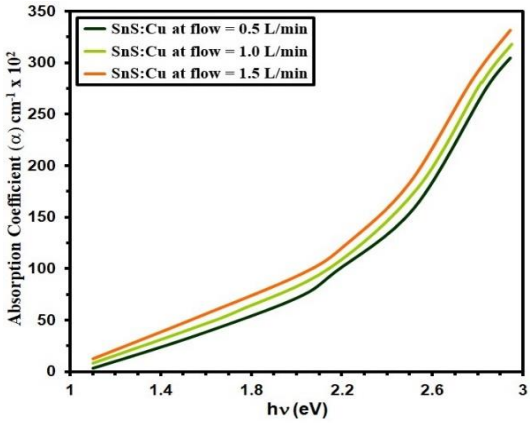

Figure 5: α of SnS: Cu films.

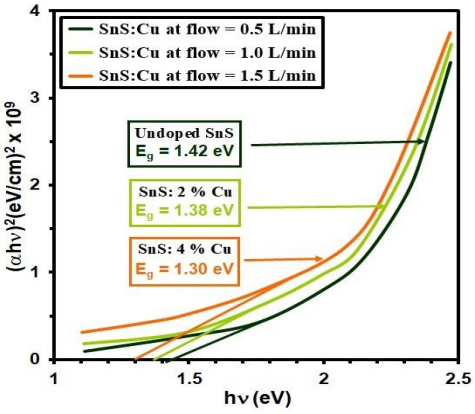

Figure 6: Eg value of SnS: Cu films.

The extinction coefficient (k) was calculated using the standard optical relation [44], [45], and its

variation with wavelength is shown in Figure 7. The results indicate that k decreases as the argon flow rate increases. This trend suggests that higher plasma flow during deposition reduces the material's optical losses, which is consistent with improved film quality and reduced defect-related absorption [46], [47].

The refractive index (n) was evaluated using the established relation that incorporates both reflectance and extinction coefficient [48], [49]. Its spectral dependence is illustrated in Figure 8. The results show a decreasing trend of n with increasing argon flow rate [50], [51]. This behavior may be explained by structural and electronic modifications induced by enhanced plasma–solution interactions, which can reduce film density and alter the optical response of the material [52], [53].

Figure 9 presents the time-dependent resistance response of SnS:Cu thin films exposed to 375 ppm NO_2 at 125 °C under different argon flow rates. The measurements indicate that the electrical resistance decreases as the argon flow rate increases, suggesting that higher plasma flow improves crystallinity and surface uniformity. These structural enhancements facilitate more efficient charge transport within the films, resulting in reduced overall resistance [46], [47].

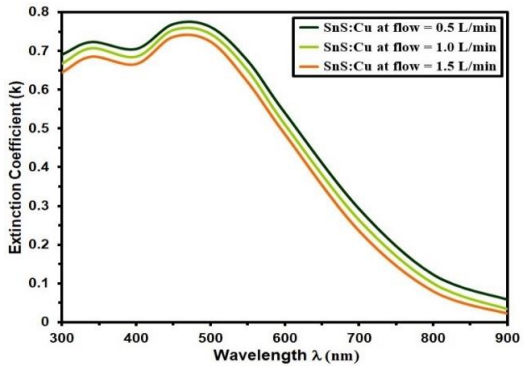

Figure 7: k of SnS: Cu films.

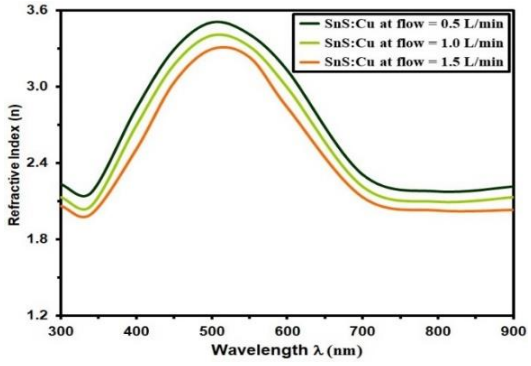

Figure 8: n of SnS: Cu films.

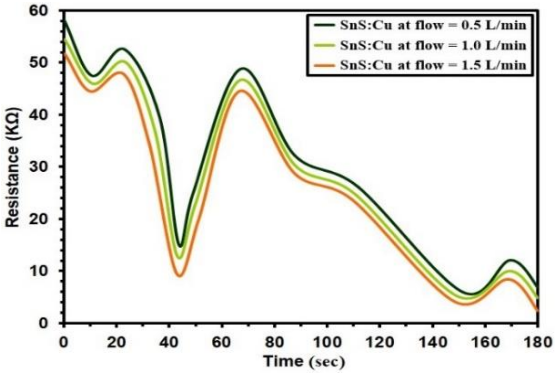

Figure 9: Resistance change over time for SnS: Cu films at different varying argon flow rates.

The gas sensor sensitivity (S) was evaluated using the standard expression [54], [55], which defines the relative change in resistance upon exposure to the target gas. In this relation, $R_a$corresponds to the resistance measured in the presence of NO_2, while $R_g$represents the baseline resistance in air. The sensitivity results of SnS:Cu thin films deposited at different argon flow rates are presented in Figure 10 for various NO_2 concentrations [56], [57].

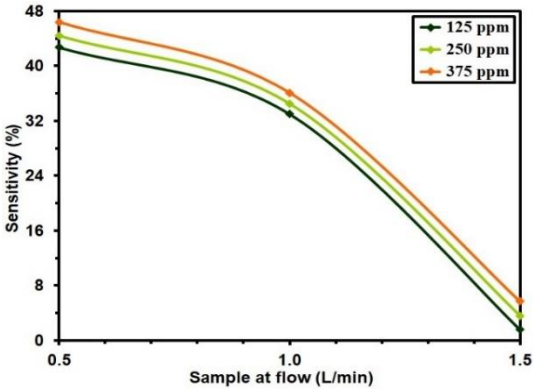

Figure 10: Sensitivity (S) of SnS: Cu films at different varying argon flow rates.

The data reveal a clear decrease in sensitivity with increasing argon flow rate. Quantitatively, the sensitivity drops from 42.70% to 1.63% at 125 ppm, from 44.41% to 3.59% at 250 ppm, and from 46.52% to 5.75% at 375 ppm. This pronounced reduction indicates that higher argon flow conditions negatively affect the gas sensing performance of the films.

This behavior can be explained by enhanced charge carrier recombination and changes in the surface properties of the material when exposed to NO_2. As the argon flow rate increases, structural modifications such as improved crystallinity and

reduced defect density may lead to fewer active adsorption sites, which ultimately weakens the interaction between the gas molecules and the film surface. As a result, the overall sensing response decreases significantly [14], [58], [59].

4 CONCLUSIONS

The plasma jet technique proved to be effective in producing high-deposition films. The SnS: Cu films exhibited a pure crystalline structure with a prominent peak along the (115) direction. Structural studies revealed an increase in the crystallite size (D) from 11.25 nm to 12.36 nm as the argon flow rate increased from 0.5 L/min to 1.5 L/min. The strain decreases from 30.81 to 28.04 as the flow rate increases. AFM images reveal that the average particle size ranges from 88.1 nm for films prepared at 0.5 L/min to 42.3 nm for those prepared at 1.5 L/min. The transmittance spectra of the films decrease from 75% to 70% as the flow rate increases. The absorption coefficient (α) increased with higher argon flow rates, while the optical gap decreased from 1.42 eV to 1.30 eV as the flow rate increased. Additionally, both the refractive index (n) and the extinction coefficient (k) decrease with increasing plasma gas flow. Increasing argon flow during deposition improves SnS:Cu film crystallinity and uniformity, enhancing charge transport and reducing overall electrical resistance. Higher argon flow rates reduce SnS:Cu film. Higher argon flow rates reduce SnS:Cu film sensitivity.

ACKNOWLEDGMENTS

The support for this paper came from Mustansiriyah University (www.uomustansiriyah.edu.iq), which the submitters wish to appreciate.

REFERENCES

[1] B.J. Lokhande, P.S. Patil and M.D. Uplane, “Studies on structural, optical and electrical properties of boron doped zinc oxide films prepared by spray pyrolysis technique,” Phys. B, vol. 302/303, pp. 59-63, 2001.

[2] N. Koteeswara Reddy and K.T. Ramakrishna Reddy, “,” Mater. Chem. Phys., vol. 102, pp. 13-18, 2007.

[3] P. Sinsermsuksakul, K. Hartman, S. B. Kim, J. Heo, L. Sun, H. H. Park, R. Chakraborty, T. Buonassisi, and R. G. Gordon, “,” Appl. Phys. Lett., vol. 102, 053901, 2013.

[4] C. Letters, E. Guneri, F. Gode, C. Ulutas, F. Kirmizigul, G. Altindemir, and C. Gumus, “Properties of P-Type SnS Thin Films Prepare by Chimica Bath Deposition,” Chalcogenide Lett., vol. 7, pp. 685-694, 2011.

[5] L. Ehm, K. Knorr, P. Dera, A. Krimmel, P. Bouvier, and M. Mezouar, “,” Journal of Physics: Condensed Matter, vol. 92, 161, 2004.

[6] A. Javed, Q. Ain and M. Bashir, “Controlled growth, structure and optical properties of Fe-doped cubic π-SnS thin films,” J. Alloy. Compd., vol. 759, pp. 14-21, 2018.

[7] S.S. Hegde, A.G. Kunjomana, K. Ramesh, K.A. Chandrasekharan, and M. Prashantha, “Preparation and characterization of SnS thin films for solar cell application,” Int. J. Soft Comput. Eng., vol. 1, pp. 38-44, 2011.

[8] M.M. El-Nahass, H.M. Zeyada, M.S. Aziz, and N.A. El-Ghamaz, “Optical properties of thermally evaporated SnS thin films,” Opt. Mater., vol. 20, pp. 159-170, 2002.

[9] Y. Guo, W. Shi, Y. Zhang, L. Wang, and G. Wei, “Investigations on Sb2O3 doped-SnS thin films prepared by vacuum evaporation,” Proc. SPIE, vol. 69841, pp. Q1-Q4, 2008.

[10] S.M. Ahmed, L.A. Latif and A.K. Salim, “The effect of substrate temperature on the optical and structural properties of tin sulfide thin films,” J. Basrah Res. Sci., vol. 37, pp. 1-7, 2011.

[11] R. Mariappan, T. Mahalingam and V. Ponnuswamy, “Preparation and characterization of electrodeposited SnS thin films,” Optik, vol. 122, pp. 2216-2219, 2011.

[12] Y.H. Gu, Y.Y. Gu, W.M. Shi, Y.H. Qian and G.P. Wang, “Influence of In-doping on resistivity of chemical bath deposited SnS films,” J. Shanghai Univ., vol. 11, pp. 403-406, 2007.

[13] E. Guneri, F. Gode, C. Ulutas, F. Kirmizigul, G. Altindemir and C. Gumus, “Properties of p-type SnS thin films prepared by chemical bath deposition,” Chalcogenide Lett., vol. 7, pp. 685-694, 2010.

[14] A. Akkari, C. Guasch and N. Kamoun-Turki, “Chemically deposited tin sulphide,” J. Alloys Comp., vol. 490, pp. 180-183, 2010.

[15] Tanusevski and D. Poelman, “Optical and photoconductive properties of SnS thin films prepared by electron beam evaporation,” Sol. Energy Mater. Sol. Cells, vol. 80, pp. 297-303, 2003.

[16] K. Hartman, J.L. Johnson, M.I. Bertoni, D. Recht, M.J. Aziz, M.A. Scarpulla and T. Buonassisi, “SnS thin films by RF sputtering at room temperature,” Thin Solid Films, vol. 519, pp. 7421-7424, 2011.

[17] M.A. Issa and K.A. Aadim, “Study the structural and optical properties of Zinc Oxide prepared by pulse laser deposition,” J. Opt., 2024, [Online]. Available: https://doi.org/10.1007/s12596-024-02034-2.

[18] M.A. Issa and K.A. Aadim, “Optical and structural characterization of ZnO:NiO nano composite prepared by pulsed laser deposition method,” J. Opt., vol. 54, pp. 2357-2362, 2025, [Online]. Available: https://doi.org/10.1007/s12596-024-01951-6.

[19] M.A. Issa and K.A. Aadim, “Influence of laser energy on structural and optical properties of ZnO(x):NiO(1−x) films prepared by pulse laser deposition,” J. Opt., 2024, [Online]. Available: https://doi.org/10.1007/s12596-024-02212-2.

[20] S.C. Ray, K.K. Malay and D. DasGupta, "Structure and photoconductive properties of dip-deposited SnS and SnS2 thin films," Thin Solid Films, vol. 350, pp. 72-78, 1999.

[21] S.S. Chiad and T.H. Mubarak, "The effect of Ti on physical properties of Fe2O3 thin films for gas sensor applications," Int. J. Nanoelectron. Mater., vol. 13, no. 2, pp. 221-232, 2020.

[22] K.N. Reddy and K.T.R. Reddy, "Optical behaviour of sprayed tin sulphide thin films," Mater. Res. Bull., vol. 41, pp. 414-422, 2006.

[23] I.B. Kherchachi, A. Attaf, H. Saidi, A. Bouhdjer, H. Bendjedidi, Y. Benkhetta, and R. Azizi, "Structural, optical and electrical properties of SnxSy thin films grown by spray ultrasonic," J. Semicond., vol. 37, 032001, 2016.

[24] B.G. Jeyaparkash, A. Amalarani, K. Kesavan and S. Mohan, "Characterization of microwave assisted chemically deposited SnS thin film," Chalcogenide Lett., vol. 6, no. 9, p. 455, 2009.

[25] M.H. Albanda Al-Timimi, W.H. Abdullah and M.Z., "Influence of thickness on some physical characterization for nanostructured MgO thin films," East Eur. J. Phys., no. 2, pp. 173-181, 2023.

[26] Y. Guo, W. Shi, Y. Zhang, L. Wang and G. Wei, "Influence of substrate temperature on properties of tin sulfide thin films," Proc. SPIE, vol. 6984, pp. 6984-1, 2008.

[27] R.S. Ali, M.K. Mohammed, A.A. Khadayeir, Z.M. Abood, N.F. Habubi and S.S. Chiad, "Structural and optical characterization of sprayed nanostructured indium doped Fe2O3 thin films," J. Phys.: Conf. Ser., vol. 1664, 012001, 2020.

[28] R. Kuekha, T.H. Mubarak and B. Azhdar, "Synthesis, structural, magnetic, and dielectric properties of Ni2+, Mn2+ co-substituted CoFe2O4 nanoferrites using sol–gel auto combustion method," Mater. Sci. Eng. B, vol. 292, 116411, 2023.

[29] N.K. Reddy, K. Ramesh, R. Ganesan, R.K.T. Ramakrishna, K.R. Gunasekhar and E.S.R. Gopal, "Synthesis and characterisation of coevaporated tin sulphide thin films," Appl. Phys. A, vol. 83, no. 1, p. 133, 2006.

[30] Cifuentes, M. Botero, E. Romero, C. Calderon and G. Gordillo, "Optical and structural studies on SnS films grown by co-evaporation," Braz. J. Phys., vol. 36, no. 3B, p. 1046, 2006.

[31] M. Devika, R.K.T. Ramakrishna, N.K. Reddy, et al., "Microstructure dependent physical properties of evaporated tin sulfide films," J. Appl. Phys., vol. 100, 023518, 2006.

[32] B.A. Bader, S.K. Muhammad, A.M. Jabbar, K.H. Abass, S.S. Chiad and N.F. Habubi, "Synthesis and characterization of indium-doped CdO nanostructured thin films," J. Nanostruct., vol. 10, no. 4, pp. 744-750, 2020.

[33] H. Noguchi, A. Setiyadi, H. Tanamura, T. Nagatomo and O. Omoto, "Characterization of vacuum evaporated tin sulfide film for solar cell materials," Sol. Energy Mater. Sol. Cells, vol. 35, p. 32, 1994.

[34] Subramaniana, C. Sanjeeviraja and M. Jayachandrana, "Photo electrochemical characteristics of brush plated tin sulfide thin films," Sol. Energy Mater. Sol. Cells, vol. 79, p. 57, 2003.

[35] A.A. Khadayeir, R.I. Jasim, S.H. Jumaah, N.F. Habubi and S.S. Chiad, "Influence of substrate temperature on physical properties of nanostructured ZnS thin films," J. Phys.: Conf. Ser., vol. 1664, 2020.

[36] M.S. Selim, M.E. Gouda, M.G. El-Shaarawy, A.M. Salema and W.A. Abd El-Ghany, "Effect of thickness on optical properties of thermally evaporated SnS films," J. Appl. Sci. Res., vol. 7, no. 6, p. 955, 2011.

[37] Guneri, C. Ulutas, F. Kirmizigul, G. Altindemir, F. Gode and C. Gumus, "Effect of deposition time on structural, electrical and optical properties of SnS thin films," Appl. Surf. Sci., vol. 257, p. 1189, 2010.

[38] N.Y. Ahmed, B.A. Bader, M.Y. Slewa, N.F. Habubi and S.S. Chiad, "Effect of boron on structural and optical characterization of nanostructured Fe2O3 thin films," NeuroQuantology, vol. 18, no. 6, pp. 55-60, 2020.

[39] Y. Wang, Y. Reddy and H. Gong, "Large-surface-area nanowall SnS films prepared by chemical bath deposition," J. Electrochem. Soc., vol. 156, no. 3, p. H157, 2009.

[40] Turan, M. Kul, A.S. Aybek and M. Zor, "Structural and optical properties of SnS semiconductor films produced by chemical bath deposition," J. Phys. D: Appl. Phys., vol. 42, 245408, 2009.

[41] D. Avellaneda, M.T.S. Nair and P. K. Nair, "Photovoltaic structures using chemically deposited tin sulfide thin films," Thin Solid Films, vol. 517, p. 2500, 2009.

[42] Hodes, Chemical Solution Deposition of Semiconductor Films, New York, NY, USA: Marcel Dekker, 2003.

[43] P. Pramanik, P.K. Basu and S. Biswas, "Preparation and characterization of chemically deposited tin(II) sulphide thin films," Thin Solid Films, vol. 150, p. 269, 1987.

[44] D. Avellaneda, M.T.S. Nair and P. K. Nair, "Polymorphic tin sulfide thin films of zinc blende and orthorhombic structures," J. Electrochem. Soc., vol. 155, no. 7, p. D517, 2008.

[45] P.P. Hankare, A.V. Jadhav, P.A. Chate, K.C. Rathod, P.A. Chavan and S.A. Ingole, "Synthesis and characterization of tin sulfide thin films grown by chemical bath deposition," J. Alloys Comp., vol. 463, no. 1-2, p. 581, 2008.

[46] A.A. Khadayeir, E.S. Hassan, T.H. Mubarak, S. S. Chiad, N.F. Habubi, M.O. Dawood and I.A. Al-Baidhany, "The effect of substrate temperature on the physical properties of copper oxide films," J. Phys.: Conf. Ser., vol. 1294, 022009, 2019.

[47] D. Avellaneda, G. Delgado, M.T.S. Nair and P.K. Nair, "Structural and chemical transformations in SnS thin films," Thin Solid Films, vol. 515, p. 5771, 2007.

[48] J. Xu, G. Wei, W. Shi, P. Chen and Y. Xue, "Preparation and characterization of chemically deposited SnS thin films," Proc. SPIE, vol. 5774, p. 254, 2004.

[49] H.H. Park, R. Heasley, L. Sun, V. Steinmann, R. Jaramillo, K. Hartman, R. Chakraborty, P. Sinsermsuksakul, D. Chua, T. Buonassisi and R.G. Gordon, "Co-optimization of SnS absorber and Zn(O,S) buffer materials for improved solar cells," Prog. Photovolt. Res. Appl., vol. 23, pp. 901-908, 2015.

[50] B.K. Pandey and R. Gopal, “Synthesis and Mn doped band gap engineering in SnS nanoparticles,” Mater. Lett., vol. 272, pp. 127840-127852, 2020.

[51] P.C. Huang, M.O. Shaikh and S.C. Wang, “Structural and optoelectronic properties of alloyed SnxMn1-xS thin films,” Adv. Powder Technol., vol. 27, no. 3, pp. 964-970, 2016.

[52] Zhang, Y. Balaji, N. Mehta, M. Heyns, M. Caymax, I. Radu and A. Delabie, “Formation mechanism of 2D SnS2 and SnS by chemical vapor deposition using SnCl4 and H2S,” pp. 6172-6178, 2018.

[53] P. Sinsermsuksakul, R. Chakraborty, S.B. Kim, S.M. Heald, T. Buonassisi and R.G. Gordon, “Antimony-doped tin(II) sulfide thin films,” Chem. Mater., vol. 24, pp. 4556-4562, 2012.

[54] A. Chowdhury, B. Biswas, M. Majumder, M.K. Sanyal and B. Mallik, “Studies on phase transformation and molecular orientation in nanostructured zinc phthalocyanine thin films,” Thin Solid Films, vol. 520, pp. 6695-6704, 2012.

[55] M. Sudha and P. Duraisamy, “Optical and structural studies on SnS thin films grown by spray pyrolysis technique,” J. Optoelectron. Adv. Mater., vol. 11, pp. 999-1003, 2012.

[56] M. Devika, N.K. Reddy, F. Patolsky and K.R. Gunashekhar, “Ohmic contacts to SnS films,” J. Appl. Phys., vol. 104, 124503, 2008.

[57] M. Devika, N.K. Reddy, R.D. Sreekantha, et al., “Synthesis and characterization of nanocrystalline SnS films,” J. Electrochem. Soc., vol. 155, no. 2, p. H130, 2008.

[58] M. Devika, N.K. Reddy, K. Ramesh, et al., “The effect of substrate surface on the physical properties of SnS films,” Semicond. Sci. Technol., vol. 21, p. 1495, 2006.

[59] M. Jayachandran, S. Mohan, B. Subramanian, C. Sanjeeviraja and V. Ganeshan, “Studies on the brush plated SnS thin films,” J. Mater. Sci. Lett., vol. 20, p. 381, 2000.